SENSOR LETTERS
Vol. 16, 1–9, 2018

Utilization of Powdered Eggshell Waste for Rhodamine B Removal: Evaluation of Adsorptive Efficiencies and Modeling Studies

Wahiba Bessashia[1,2], Zhour Hattab[2], Yamina Berredjem[1], Ridha Djellabi[2,*], Radia Zerdoum[1], Assia Allaoui[2], Abdelhak Gheid[1], and Kamel Guerfi[2]

[1] *Science and Technology Laboratory of Water and Environment, Mohammed Cherif Messadia University, Souk Ahras 41000, Algeria*
[2] *Laboratory of Water Treatment and Valorization of Industrial Wastes, Badji-Mokhtar University, Annaba 23000, Algeria*

(Received: 3 February 2018. Accepted: 3 February 2018)

Biomass wastes are being recognized as emerging functional platforms that can be utilized in various fields. Eggshell, which can be found everywhere due to the large eggs consumption, has usually been regarded as waste and overlooked. In this contribution, we report the use of three powders prepared from eggshell waste such as Eggshell without membrane (ES), Eggshell membrane (ESM) and Eggshell with membrane (ESM-ES) as biosorbents for the removal of Rhodamine B (RhB) from water. Biosorbent powders were characterized by XRD, SEM, BET and FTIR. The effects of initial RhB concentration, temperature and pH on dye adsorption were performed. The results showed that the ESM, due to its 3D network porous structure, exhibited the highest adsorption efficiency than ES and ES-ESM. The RhB sorption on these adsorbents obeys pseudo-second-order kinetics which indicates a chemisorption process. For ESM adsorbent, the Freundlich isotherm model has a best-fit compared to Langmuir and Temkin isotherm models (multilayer dye adsorption with non-uniform distribution). However, for ES and ESM-ES adsorbents Langmuir has a best-fit than the other models (monolayer dye adsorption).

Keywords: Biomaterial Recycling, Eggshell Waste, Rhodamine B Removal, Adsorption, Environmental.

RESEARCH ARTICLE

1. INTRODUCTION

Due to the dramatic increase in population growth, agricultural and industrialization activities, water demand has increased up to nine-fold in the 20th century.[1] Many countries are expected to face water crisis in the next decades. Thereby, water purification and reuse have become one of the major global concerns in scientific community. Researchers are developing water purification technologies that might be environmental friendly, economical and efficient for each kind of industrial wastewaters. Dyes and pigments industries use an extensive amount of waters in their manufacturing processes. Wastewaters from such industries are classified as the most polluting of all the industrial sectors, considering the amount produced as well as the physicochemical composition of their effluents which cause severe pollution problems in current times.[2,3] It is know that dyes and pigments usually are designed to resist biodegradation, as a result they can remain in the environment for a long period of time.[4,5] Consequently, the removal of color of dyes and pigments from wastewaters is one of the most difficult tasks confronted by the wastewater treatment plants. On the other side, the environment protection authorities highly encourage the sustainable management of solid wastes for beneficial reuse in different fields. Recently, exploring novel industrial solid wastes and natural materials is of growing interest in the field of environment remediation due to their low-cost and their different physicochemical properties. Certainly, to support the beneficial reuse, materials should be used depending on their characteristics for a specific target application. Therefore due to development in adsorption, numerous waste-based adsorbents

*Corresponding author; E-mail: ridha.djellabi@yahoo.com

are being investigated for dyes adsorption such as orange peel activated carbon for Direct N Blue-106 adsorption,[6] sugar beet pulp for Gemazol turquoise blue-G adsorption,[7] powdered peanut hull for Sunset yellow, Amaranth and Fast green adsorption,[8] rice husk ash for Indigo Carmine adsorption,[9] peanut hull for Methylene blue, Brilliant cresyl blue and Neutral red adsorption,[10] coir pith carbon for Methylene blue adsorption,[11] tea waste for Methylene blue adsorption,[12] coniferous pinus bark powder for Crystal violet adsorption,[13] lemon peel for Malachite green adsorption,[14] bagasse fly ash for Methyl violet adsorption,[15] almond shells for Direct red 80 adsorption[16] and neem sawdust for Malachite green adsorption.[17] One of the alternative adsorbent materials for dyes removal from water is eggshell waste. Eggshell waste has usually been overlooked which cases its accumulation in the environment. Zhang et al. reported that over 10^{12} eggs are consumed worldwide annually.[18] Eggshell (ES) is a hard shell composed mainly of calcite, while eggshell membrane (ESM) is the protein-rich membrane with highly cross-linked fibers found between the ES and egg white. ESM has an important role in the mineralization of ES and the albumen due to its water and gas permeability.[19] It is a non-toxic porous biomass material with special functional groups such as –OH, –SH, –COOH and $–NH_2$, that could be great promise as a biosorbent for dyes removal from water. Aim of this work was to explore eggshell and eggshell membrane s biosorbents to remove Rhodamine from water. ES, ESM and ES-ESM powders were prepared and characterized by SEM, BET, FTIR and XRD. The effects of some parameters on the sorbing efficiency were investigated. The equilibrium data were analysed using three adsorption isotherm models: Langmuir, Freundlich and Temkin, while the adsorption kinetics was followed by pseudo-first order and pseudo-second order.

2. EXPERIMENTAL DETAILS

2.1. Materials

All the chemicals used were of analytical grad and purchased from Sigma-Aldrich-Fluka. RhB solution was prepared by dissolving of an accurately weighed amount in bidistilled water and subsequently diluted to required concentrations. Chicken eggshell waste was obtained from local restaurants.

2.2. Methods

2.2.1. Preparation of ESM, ES and ES-ESM Powders

Eggshell was washed several times with bidistilled water and HCl and then was boiled in distilled water to remove residual impurities. Afterwards, ESM was carefully stripped from the ES manually. Subsequently, both ES and ESM were washed with running bidistilled water and dried an oven at 80 °C overnight. ES and ESM were then crushed in order to achieve powder form and only the particles of size between 0.07 and 0.1 mm were used.

Fig. 1. Preparation of ESM, ES and ES-ESM.

On the other hand, full ES (the material was used as is it, with membrane) powder was also prepared using the same steps. Figure 1 summarizes the steps used to prepare different powders.

2.2.2. Characterization Analysis

Scanning Electron Microscope (SEM) was used to determine the morphology structure of ESM, ES and ES-ESM using JEM-2010-JEOL instrument. X-ray diffraction (XRD) data were obtained over the range of 10–80° with Cu Ka radiation using Philips X'Pert X-ray diffractometer. BET surface area analysis was performed using a Nova Quantachrome Surface Area and Porosity Analyzer. Fourier Transform Infrared analysis (FTIR) was recorded to identify the functional groups of ESM, ES and ES-ESM using the IR Affinity-1S (SHIMADZU) in combination with a single reflection ATR using a maximum pressure of 0.1 GPa, standard resolution 4 cm^{-1} and an accumulation number of 50.

2.2.3. Adsorption Tests

Batch adsorption experiments were carried out by adding a fixed amount of each adsorbent (2 g) into a number of 250 mL Erlenmeyer flasks containing 100 mL of fixed initial RhB concentration. The pH was adjusted by adding HCl (0.1 M) or NaOH (0.1 M). Then, the flasks were shacked at 150 rpm for 1 h. At equilibrium, RhB concentration was determined by absorbance measurement using UV-Vis spectrophotometer (JENWAL 7315) at 554 nm. The removal rate (R) and the amount of sorption at

RESEARCH ARTICLE

equilibrium time (q_e) were calculated according to the following equations:

$$R(\%) = \frac{C_0 - C_e}{C_0} \times 100 \quad (1)$$

$$q_e = \frac{V(C_0 - C_e)}{m} \quad (2)$$

Where C_0 (mg/L) is the initial concentration of RhB, C_e (mg/L) is the equilibrium concentration of RhB, V (L) is the volume of the RhB solution, and m (g) is the adsorbent mass.

2.2.4. Modeling of RhB Adsorption Isotherms and Kinetics

2.2.4.1. Adsorption Isotherms. Three equilibrium isotherm models were used to describe the experimental adsorption capacity of the adsorbents in batch mode.

—Langmuir model

The Langmuir adsorption model describes quantitatively the formation of a monolayer adsorbate on the outer surface of the adsorbent (the adsorbed layer is one molecule in thickness), and after that no further adsorption takes place. Thereby, the Langmuir represents the equilibrium distribution of adsorbate species between the solid and liquid phases. The adsorption can only occur at fixed number of definite localized identical and equivalent sites, without lateral interactions between the adsorbed molecules (homogeneous adsorption).[20]

Based upon these assumptions, Langmuir isotherm is expressed by the following equation:

$$\frac{1}{q_e} = \frac{1}{K_L q_m C_e} + \frac{1}{q_m} \quad (3)$$

Where q_e is the amount of the solute adsorbed per unit weight of the adsorbent at equilibrium (mg/g), C_e is the equilibrium concentration of the solute (mg/L), q_m is the maximum monolayer coverage capacity (mg/g); K_L is the Langmuir isotherm constant (L/mg).

—Freundlich model

The Freundlich isotherm is an empirical equation which is the most widely used isotherm for the explanation of adsorption equilibrium which describes the non-ideal and reversible adsorption, not restricted to the formation of monolayer. The Freundlich isotherm assumes that a multilayer adsorption can occur and that sorption can infinitely increase with increase in the aqueous concentration, with non-uniform distribution of adsorption (heterogeneous adsorption).[20] The Freundlich isotherm is expressed as:

$$\ln q_e = \ln k_F + \frac{1}{n} \ln C_e \quad (4)$$

Where k_F is Freundlich isotherm constant (mg/g; n is adsorption intensity.

—Temkin model

Temkin isotherm contains a factor that explicitly taking into the account of adsorbent–adsorbate interactions. By ignoring the extremely low and large value of concentrations, the model assumes that heat of adsorption (function of temperature) of all molecules in the layer would decrease linearly rather than logarithmic with coverage. The model is given by the following equation:

$$q_e = B_T \ln A_T + B_T \ln \, C_e \quad (5)$$

A_T is Temkin isotherm equilibrium binding constant (L/g), $B_T = RT/b$ is Temkin isotherm constant, b constant related to heat of sorption (J/mol), R is universal gas constant (8.314 J/mol/K), T is the temperature at 298 K.

2.2.4.2. Kinetic Models. Kinetic models are used to identify the adsorption mechanism type in a test system, and its potential rate-controlling steps that include mass transport and chemical reaction processes. In addition, kinetics studies are necessary to define the optimum condition for full-scale batch metal removal processes.

The adsorption kinetics of RhB on ESM, ES and ESM-ES were examined by pseudo-first order (Eq. (6)) and pseudo-second order (Eq. (7)) models.

$$\ln(q_e - q_t) = \ln q_e - k_1 \quad (6)$$

$$\frac{t}{q_t} = \frac{1}{k_2 q_e^2} + \frac{t}{q_e} \quad (7)$$

Where, q_e ($\text{mg} \cdot \text{g}^{-1}$) and q_t ($\text{mg} \cdot \text{g}^{-1}$) are the adsorption capacity at equilibrium and at time t, respectively. k_1 (min^{-1}) is the pseudo-first order rate constant. The values of k_1 and q_e, obtained from the slope and the intercept of plots of $\log(q_e - q_t)$ versus t. k_2 ($\text{g} \cdot \text{mg}^{-1} \cdot \text{min}^{-1}$) denotes the pseudo-second order rate constant. The values of k_2 and q_e were calculated from the slope and intercept of plots of t/q_t versus t.

3. RESULTS AND DISCUSSION

3.1. Characterization

3.1.1. FTIR

FTIR spectra of ESM (a), ES (b) and ESM-ES (c) are presented in Figure 2. ESM shows absorption intense peaks at 1640 and 1530 cm^{-1} which are attributed to amide C═O stretching and amide N–H bending respectively. Bands at around 1410, 1237, 663 cm^{-1} are due to CH_2 scissoring, amine C–N stretching and C–S variation respectively. Band evidenced at 3280 cm^{-1} corresponds to O–H stretching mode. Bands at around 3000 and 2900 cm^{-1} are due to the asymmetric stretching vibrations of C–H present in organic matter group,[21] while band at around 2300 cm^{-1} is attributed to C–H stretching vibration.

In the case of ES, the spectrum exhibits the same characteristic bands as a typical calcite. Intense peaks at 1402, 872 and 716 cm^{-1} are due to the vibration of CO_3^{2-} species corresponding to asymmetric stretch, the out-of

RESEARCH ARTICLE

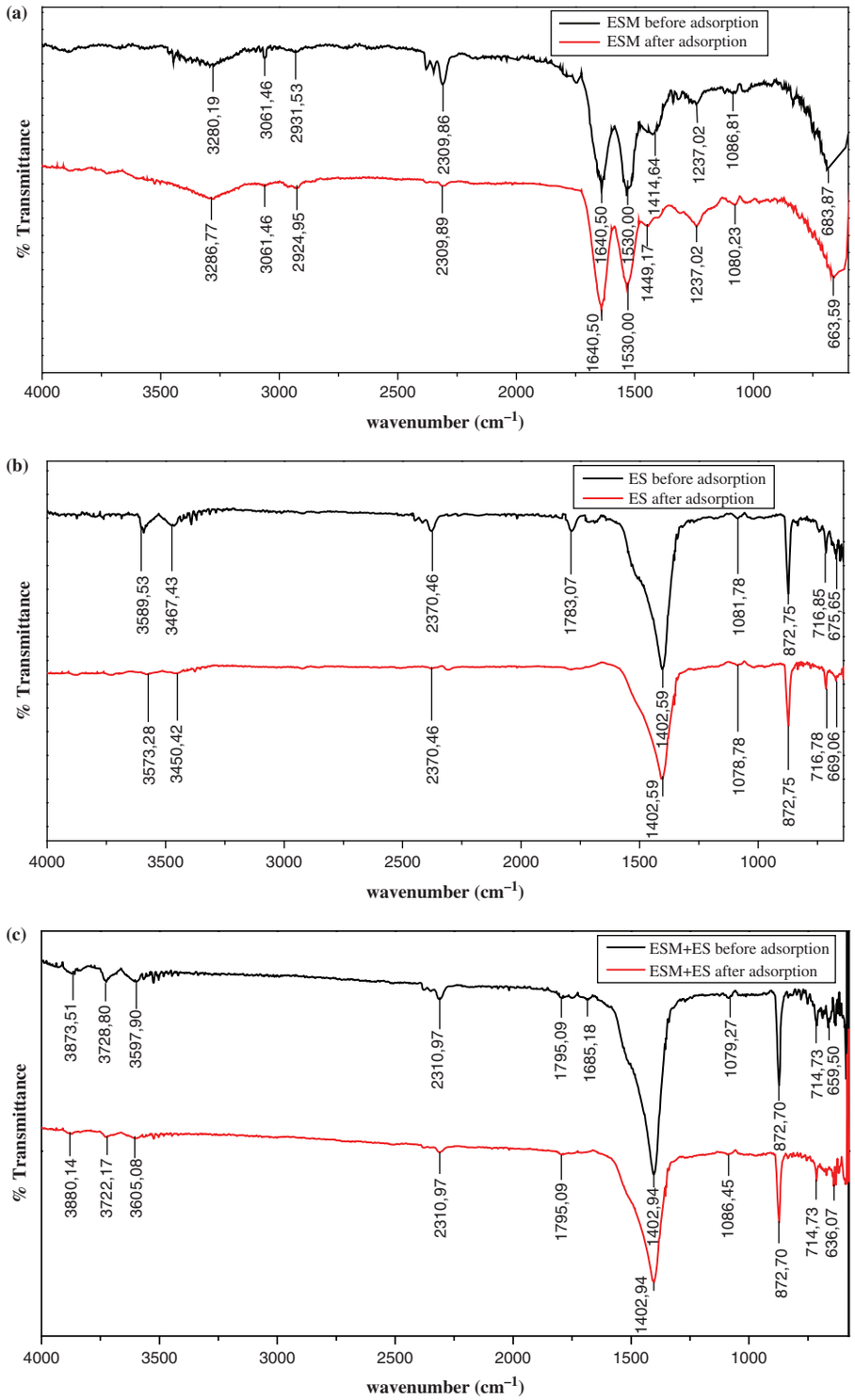

Fig. 2. FTIR spectra before and after adsorption of (a) ESM, (b) ES and (c) ESM-ES.

plane bend and in-plane bend vibration modes respectively. Small band at 1783 cm^{-1} is attributed to C═O stretching vibration. Bands at around 3400 and 3600 cm^{-1} are due to the stretching vibration of structural water species. The absorption band situated at around 2300 cm^{-1} is attributed to organic matter C–H stretching vibration. In the spectrum of ESM-ES, very similar peaks as ES were detected which due to the larger amount of ES in the

mixture compared to ESM. Besides, the band at 1402 cm^{-1} is more intense in ESM-ES spectrum.

After RhB adsorption, some changing in all spectra was occurred. In ESM spectrum, the intense peak at 1530 cm^{-1} decreases and bands at around 1410 and 2300 cm^{-1} almost disappeared. In ES and ESM-ES spectra, peaks at 1783, 2300, 3400 and 3600 cm^{-1} completely disappeared. This can be explained by the surface-dye molecules interactions such as the exchange reaction between the dye molecules and H^+ of functional groups which indicates that there was a chimisorption process.

3.1.2. SEM and BET

Figure 3 depicts SEM images of ESM, ES and ESM-ES. ESM shows 3D network structure formed by intercrossed nano/micro scale fibers arranged without specific direction that extend for long distances. These fibers form a heterogeneous surface with nano/microporous. The pore size between the fibers was obtained by BET analysis within the range of 12–22 Å. Furthermore, the specific surface area of ESM is 11.40 $m^2 \cdot g^{-1}$. SEM image of ES shows that the surface of ES is rough and sharp. In addition, nanoporous can be observed. Moreover, he specific surface area of ES is 1.88 $m^2 \cdot g^{-1}$ with an average pore size of 11 Å. SEM image of ESM-ES shows that the ES content is the main component. Some fibers are also observed but there is no interaction between ESM and ES. The specific surface area of ES is 0.783 $m^2 \cdot g^{-1}$ with an average pore size of around 11 Å.

Figure 4 illustrates SEM images of samples (at 100 μm) before and after adsorption. It can be noticed that the covering of surface by RhB molecules is evident especially in the case of ESM where multilayers of adsorbed dye are clearly observed.

3.1.3. XRD

Figure 5 illustrates XRD patterns of ESM, ES and ESM-ES. XRD pattern of ESM shows a broad peak at around $2\theta = 21°$, ascribed to the succession and conformations of amino acids in ESM, which indicates the amorphous nature of ESM. In the case of ES and ESM-ES patters, as expected, the calcite was the only mineral phase identified in XRD pattern. However, no other crystalline mineral species was detected which may be due to their low amount (under the detection limit of the XRD technique).

3.2. Adsorption of RhB

3.2.1. Effect of RhB Concentration and Kinetics of Adsorption

The effect of initial RhB concentration on the adsorption process was evaluated in the range 10–30 ppm at pH: 5.5 and temperature of 25 °C. Usually, the effect of the initial dye concentration parameter depends on the immediate relation between the dye concentration and the available sorbing sites of an adsorbent. The results in term of amount of adsorption and removal rate are illustrated in Table I and Figure 6. It can be seen that the ESM shows higher adsorption efficiency than ES and ES-ESM. This is justified the porous nature and the higher surface area of ESM compared with ES and ES-ESM. In addition, functional groups such as amine and carboxyl groups present in ESM can react with RhB molecules which results in better fixation of RhB onto the surface. On the other hand, there was a sharp increase in the amount of RhB adsorbed along with the increase of initial RhB concentration especially in the case of ESM. The amount of RhB adsorbed increased from 0.408 to 1.251 mg/g as the RhB concentration was increased from 10 to 30 ppm. This is due to the high driving force for mass transfer between the solution and the adsorbent surface at a high initial RhB concentration. It worth noting that, the increase in RhB initial concentration does not affect the removal percentage for ESM and ES as showed in Table I. Removal percentages were within the range 81–84% and 27–30% for ESM and ES respectively at different concentrations (10–30 ppm). However, a decrease in the percentage of removal with RhB concentration increasing was found in the case of ES-ESM.

The adsorption kinetics study demonstrates how the dye uptake rate and obviously this rate controls the residence time of the dye molecules at the solution interface.

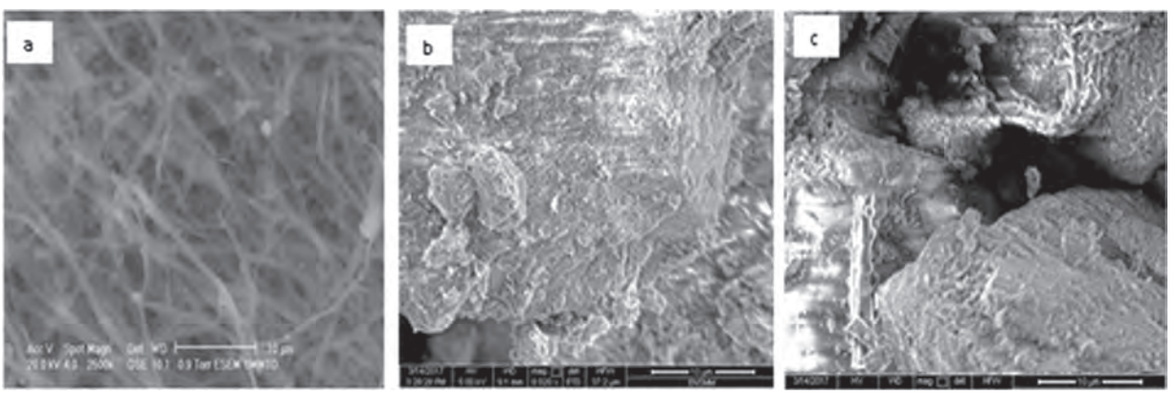

Fig. 3. SEM images of samples (at 10 μm), (a) ESM, (b) ES and (c) ESM-ES.

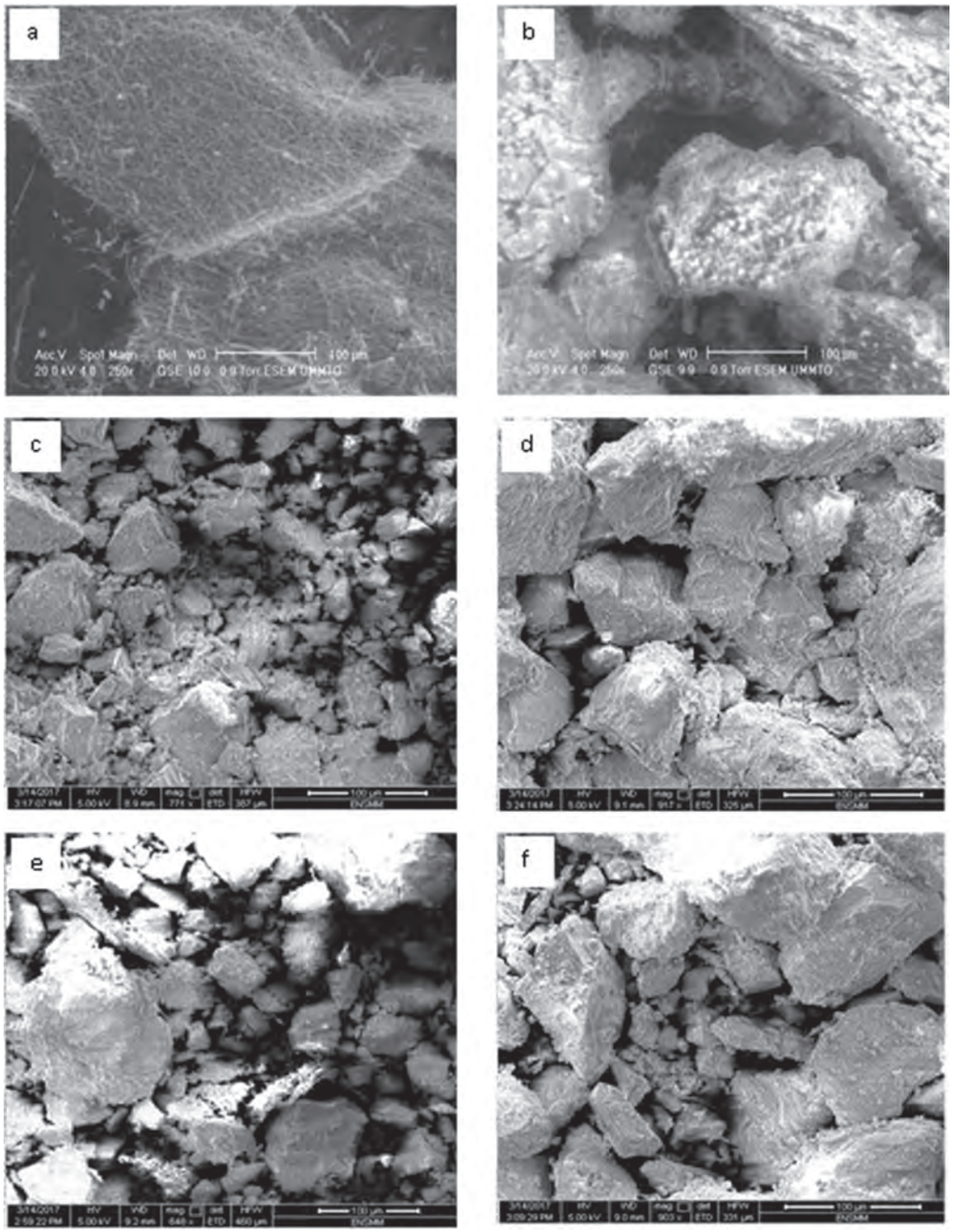

Fig. 4. SEM images of samples (at 100 μm) before and after adsorption; (a) ESM before adsorption, (b) ESM after adsorption, (c) ES before adsorption, (d) ES after adsorption, (e) ESM-ES before adsorption, (f) ESM-ES after adsorption.

For this purpose, most of adsorption studies use pseudo-first-order and pseudo-second-order models. Usually the best-fit model can be selected based on the linear regression correlation coefficient R^2 values. Table I lists the results of kinetic parameters for RhB adsorption by ESM, ES and ES-ESM using pseudo-first-order and pseudo-second-order models. The results show that the correlation coefficients R^2 of pseudo-second order were higher than those of pseudo-first order model for all adsorbents. In the case of ESM, R^2 values were very close to the unity (0.999). Furthermore, the q_e values estimated from pseudo-second order model were much closer to those obtained from the experiments. As a result, the adsorption of RhB on these adsorbents obeyed pseudo-second order model better which indicates that the adsorption of RhB on these adsorbents is a chemisorption process. Chemical bonds can be formed by the electrostatic attraction of functional groups in ESM (such as –OH, –SH, –COOH and $–NH_2$)

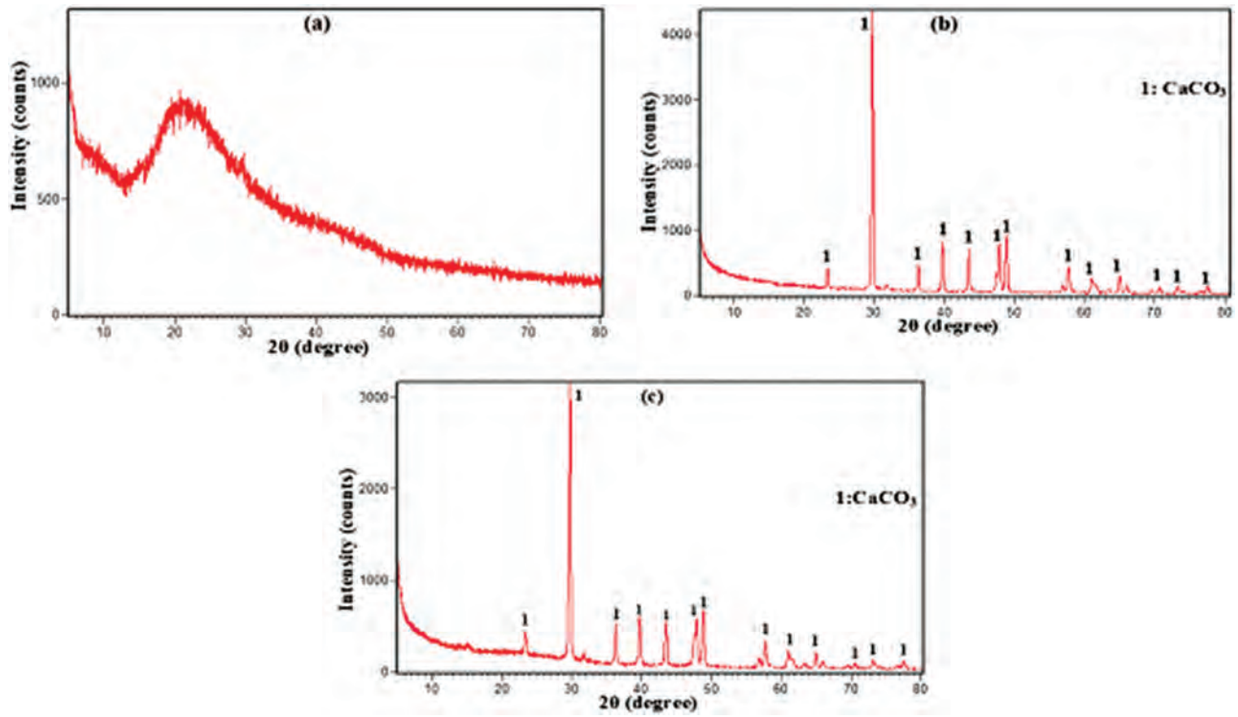

Fig. 5. XRD patterns of samples: ESM (a), ES (b), ES-ESM (c).

Table I. Effect of initial RhB concentration, temperature and pH on the adsorption efficiency.

				Pseudo-first order			Pseudo-second order		
		$q_{,\exp}$ (mg · g^{-1})	R(%)	q_e	k_1	R^2	q_e	k_2	R^2
Effect of initial RhB concentration (ppm)									
10	ESM	0.4081	81.63	0.0294	0.069	0.947	0.4020	19.21	0.999
	ES	0.1413	28.26	0.1506	0.102	0.982	0.1429	1.0836	0.965
	ESM+ ES	0.2173	43.47	0.1460	0.087	0.974	0.2171	1.4723	0.992
15	ESM	0.6160	82.13	0.0307	0.125	0.974	0.6130	23.51	0.999
	ES	0.2069	27.59	0.1101	0.136	0.967	0.1947	9.5061	0.991
	ESM + ES	0.2828	37.71	0.1364	0.065	0.965	0.2577	2.9472	0.991
20	ESM	0.8448	84.48	0.0454	0.058	0.902	0.8438	5.7787	0.999
	ES	0.3133	31.33	0.1771	0.123	0.988	0.3108	2.1384	0.996
	ESM + ES	0.3853	38.53	0.1452	0.109	0.825	0.3799	3.3041	0.998
25	ESM	1.0326	82.60	0.1045	0.191	0.975	1.01936	22.380	0.999
	ES	0.3956	31.65	0.2171	0.152	0.987	0.3770	4.2702	0.966
	ESM + ES	0.4326	34.60	0.2055	0.173	0.993	0.4122	6.4889	0.996
30	ESM	1.2519	83.46	0.0636	0.186	0.968	1.2547	9.7725	0.999
	ES	0.4565	30.43	0.1539	0.113	0.998	0.4470	3.2839	0.998
	ESM + ES	0.5149	34.32	0.1739	0.095	0.956	0.5010	2.6684	0.997
Effect of temperature (C°)									
25	ESM	0.8448	84.48	0.0454	0.058	0.902	0.8438	5.7787	0.999
35	ESM	0.8274	82.74	0.0453	0.119	0.901	0.8250	12.8880	0.999
45	ESM	0.8016	80.16	0.0249	0.064	0.873	0.7955	26.33	0.999
Effect of pH									
2	ESM	0.7961	79.61	0.0846	0.098	0.989	0.8071	2.3893	0.999
4	ESM	0.8399	83.99	0.0303	0.092	0.854	0.8438	6.4132	0.999
6	ESM	0.8423	84.23	0.0283	0.077	0.834	0.8460	6.2654	0.999
8	ESM	0.8516	85.16	0.0524	0.099	0.979	0.8583	4.0280	0.999
10	ESM	0.8627	86.27	0.0608	0.097	0.971	0.8710	0.2951	ESM

RESEARCH ARTICLE

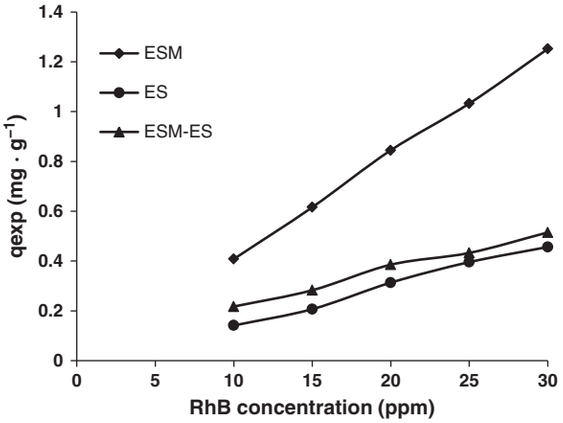

Fig. 6. Amount adsorbed of RhB as a function of initial RhB concentration for ESM, ES and ES-ESM, conditions: pH: 5.5, temperature: 25 °C, mass of adsorbent: 20 mg/L.

and RhB molecules. This behavior was proved in FTIR results. Only ESM, due to its higher adsorption efficiency, was used to carry out the effects of temperature and pH.

3.2.2. Effect of Temperature

The temperature is a significant physico-chemical process factor on the adsorption which is an indicator for the adsorption nature whether it is an exothermic or endothermic process. This effect depends mainly on the nature of the adsorbent and the movement of dye molecules of each dye class. The effect of temperature was performed by varying the temperature (25, 35 and 45 °C) at pH 6 and for an initial RhB concentration of 20 mg/L. It was found that, from the results illustrated in Table I, there was a decrease in the amount adsorbed from 0.8448 to 0.8016 mg/g as the temperature increased from 25 to 45 °C which indicates that the adsorption of RhB on ESM is an exothermic process, due to the weakening of the adsorptive forces between the RhB molecules and the active sites on the ESM adsorbent surface.

3.2.3. Effect of pH

Solution pH parameter is very important in the dye adsorption process as it controls the variation in the degree of ionization of the ionized dye molecules and the surface properties of adsorbent. The effect of initial pH on RhB adsorption onto ESM was carried out by varying the pH from 2.0 to 10 for an initial RhB concentration of 20 mg/L

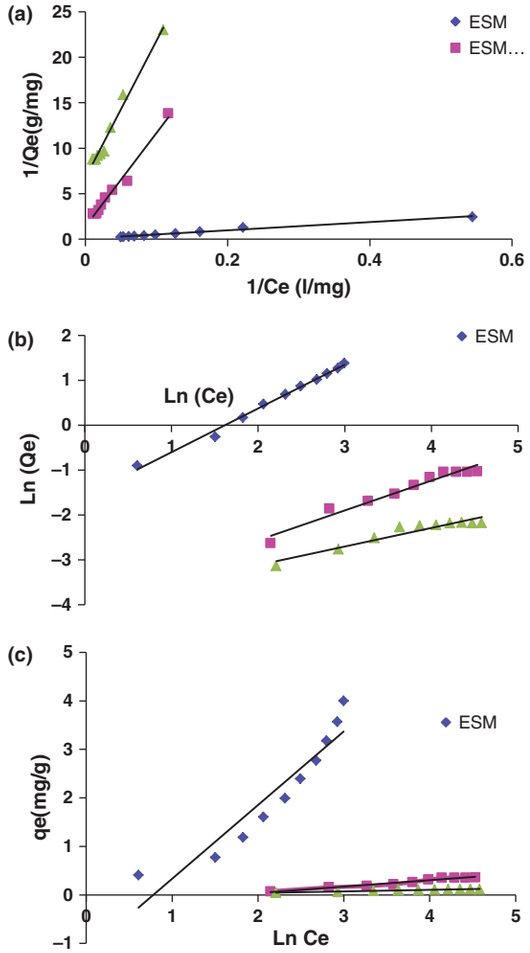

Fig. 7. Plots for Langmiur (a), Freundlich (b) and Temkin (c) isotherms for RhB adsorption on ESM, ES and ESM-ES.

at 25 °C. The results presented in Table I showed that the adsorption efficiency increased slightly with the pH increasing that could be explained by the changing of the electrostatic interactions between the surface of the adsorbent and RhB molecules. As pH decreases, the number of negatively charged sites on the adsorbent decreases and the number of positively charged sites increases, while the reverse is true.[22]

3.2.4. Adsorption Isotherm

Usually an adsorption isotherm, which is identified by certain constant values, provides information on surface

Table II. Langmuir, Freundlich and Temkin isotherm constants.

	Langmuir			Freundlich			Temkin		
Adsorbent	q_m (mg · g^{-1})	b (mg · g^{-1})	R^2	n	K_F (mg · g^{-1})	R^2	A_T (L · g^{-1})	B_T (J · mol^{-1})	R^2
ESM	14.4092	0.0153	0.9853	1.0253	0.2066	0.9930	0.4581	1.5194	0.8844
ESM-ES	0.7126	0.0136	0.9839	1.5071	0.0205	0.9587	0.1852	0.1306	0.9631
ES	0.1479	0.0448	0.9840	2.4166	0.0193	0.9138	0.4635	0.0320	0.9355

RESEARCH ARTICLE

characteristics and affinity of the adsorbent. Furthermore, it can be employed to the adsorptive capacities of the adsorbents for a pollutant. In our study, three mathematical models such as Freundlich, Langmuir and Temkin were used to analyse the adsorption occurred in the experiments. The results obtained by the application of these model equations are presented in Table II and Figure 7. For ESM adsorbent, according to the values of the regression correlation coefficient R^2, the Freundlich adsorption isotherm model has a best-fit compared to Langmuir and Temkin isotherm models. These results are consistent with the results of effect of initial dye concentration on the capacity of adsorption and SEM analysis. There was a regularly significant increase in the capacity of adsorption with the increase of initial dye concentration for ESM sample which can be due to the heterogeneous surface of ESM. In addition, SEM image of ESM after adsorption (Fig. 4(b)) shows the formation of net multilayers of adsorbed dye molecules with non-uniform distribution of adsorption, and the concentration of dye molecules on the surface was completely heterogeneous. However, for ES and ESM-ES adsorbents Langmuir has a best-fit than the other models. The occupancy ES and ESM-ES surfaces could occur at an energetically homogeneous range of adsorption sites where the surface phase may be considered as a monolayer.

4. CONCLUSION

The results of this work demonstrated that powdered eggshell waste can be employed as an alternative adsorbent for RhB removal from water. ESM exhibits a higher porosity and surface area compared with ES and ESM-ES. Therefore, ESM had twice better adsorption performances than ES and ESM-ES. The amount of RhB adsorbed was found to be increased significantly with initial RhB concentration increasing. Temperature and pH of solution had little influences on RhB adsorption onto ESM. The study of adsorption kinetics suggested that the RhB adsorption mechanism followed the pseudo-second model well which indicates that the adsorption process is chemisorption. The equilibrium analysis reflected that the Freundlich model fitted isotherm date well for ESM adsorbent. While, for ES and ESM-ES adsorbents Langmuir had a best-fit.

Acknowledgments: The authors gratefully acknowledge financial support from the Algerian Ministry of Higher Education and Scientific Research.

References and Notes

1. S. S. Shenvi, A. M. Isloor, and A. Ismail, A review on RO membrane technology: Developments and challenges. *Desalination* 368, 10 (**2015**).
2. A.-B. Dos-Santos, F.-J. Cervantes, and J. B. Van-Lier, Review paper on current technologies for decolourisation of textile wastewaters: Perspectives for anaerobic biotechnology. *Bioresour. Technol.* 98, 2369 (**2007**).
3. R. Djellabi, M. F. Ghorab, and T. Sehili, Simultaneous removal of methylene blue and hexavalent chromium from water using TiO_2/Fe(III)/sunlight. *Journal CLEAN–Soil, Air, Water* 45, 6 (**2017**).
4. O.-J. Hao, H. Kim, and P.-C. Chiang, Decolorization of wastewater. *Crit. Rev. Environ. Sci. Technol.* 30, 449 (**2000**).
5. P. Firmino, M. Silva, F. J. Cervantes, and A. B. Santos, Colour removal of dyes from synthetic and real textile wastewaters in one- and two-stage anaerobic systems. *Bioresour. Technol.* 101, 7773 (**2010**).
6. A. Khaled, A. E. Nemr, A. El-Sikaily, and O. Abdelwahab, Removal of direct N Blue-106 from artificial textile dye effluent using activated carbon from orange peel: Adsorption isotherm and kinetic studies. *J. Hazard. Mater.* 165, 100 (**2009**).
7. Z. Aksu and I. A. Isoglu, Use of agricultural waste sugar beet pulp for the removal of Gemazol turquoise blue-G reactive dye from aqueous solution. *J. Hazard. Mater.* 137, 418 (**2006**).
8. R. Gong, Y. Ding, M. Li, C. Yang, H. Liu, and Y. Sun, Utilization of powdered peanut hull as biosorbent for removal of anionic dyes from aqueous solution. *J. Dyes Pig.* 64, 187 (**2005**).
9. U. R. Lakshmi, V. C. Srivastava, I. D. Mall, and D. H. Lataye, Rice husk ash as an effective adsorbent: Evaluation of adsorptive characteristics for indigo carmine dye. *J. Environ. Manage.* 90, 710 (**2009**).
10. R. Gong, M. Li, C. Yang, Y. Sun, and J. Chen, Removal of cationic dyes from aqueous solution by adsorption on peanut hull. *J. Hazard. Mater.* 121, 247 (**2005**).
11. D. Kavitha and C. Namasivayam, Experimental and kinetic studies on methylene blue adsorption by coir pith carbon. *J. Biores. Technol.* 98, 14 (**2007**).
12. M. T. Uddin, M. A. Islam, S. Mahmud, and M. Rukanuzzaman, Adsorptive removal of methylene blue by tea waste. *J. Hazard. Mater.* 164, 53 (**2009**).
13. R. Ahmad, Studies on adsorption of crystal violet dye from aqueous solution onto coniferous pinus bark powder (CPBP). *J. Hazard. Mater.* 171, 767 (**2009**).
14. K. V. Kumar, Optimum sorption isotherm by linear and non-linear methods for malachite green onto lemon peel. *J. Dyes Pig.* 74, 595 (**2007**).
15. I. D. Mall, V. C. Srivastava, and N. K. Agarwal, Removal of orange-G and methyl violet dyes by adsorption onto bagasse fly ash—kinetic study and equilibrium isotherm analyses. *J. Dyes Pig.* 69, 210 (**2006**).
16. F. D. Ardejani, K. Badii, N. Y. Limaee, S. Z. Shafaei, and A. R. Mirhabibi, Adsorption of direct red 80 dye from aqueous solution onto almond shells: Effect of pH, initial concentration and shell type. *J. Hazard. Mater.* 151, 730 (**2008**).
17. S. D. Khattri and M. K. Singh, Removal of malachite green from dye wastewater using neem sawdust by adsorption. *J. Hazard. Mater.* 167, 1089 (**2009**).
18. D. Zhang, H. Zhao, and Z. J. Fan, A highly sensitive and selective hydrogen peroxide biosensor based on gold nanoparticles and three-dimensional porous carbonized chicken eggshell membrane. *Plos One* 10 (**2015**).
19. D. Yang, L. Qi, and J. Ma, Eggshell membrane templating of hierarchically ordered macroporous networks composed of TiO_2 tubes. *Advanced Materials* 14, 1543 (**2002**).
20. K. Y. Foo and B. H. Hameed, Insights into the modeling of adsorption isotherm system. *Chem. Eng. J.* 156, 2 (**2010**).
21. J. Choi, B. Pant, C. Lee, P. Mira, P. Soo-Jin, and K. Hak-Yong, Preparation and characterization of eggshell membrane/PVA hydrogel via electron beam irradiation technique. *Ind. Eng. Chem. Res.* 47, 41 (**2017**).
22. T. Y. Mustafa, K. S. Tushar, A. Sharmeen, and H. M. Ang, Dye and its removal from aqueous solution by adsorption: A review. *Adv. Colloid Interface Sci.* 209, 172 (**2014**).